Advances in Science and Technology Research Journal

Advances in Science and Technology Research Journal, 2026, 20(2), 171–181
https://doi.org/10.12913/22998624/211671
ISSN 2299-8624, License CC-BY 4.0

Received: 2025.10.15
Accepted: 2025.09.01
Published: 2025.12.23

Sustainable synthesis of fluorapatite from eggshells: Influence of precursor addition rate on phase purity and microstructure

Ganka Kolchakova[1*], Dimitrina Kiryakova[1]

[1] Department of Material Science, Burgas State University, Burgas, Bulgaria
[*] Corresponding author's e-mail: gkolchakova@gmail.com

ABSTRACT

This study investigated how the rate of addition of the phosphorus-fluoride precursor affects the sustainable synthesis of fluorapatite (FAp) from waste eggshells. A co-precipitation method and different precursor addition rates of 0.5 and 5 mL/min were used to determine their influence on the phase composition, crystallinity, and morphology of the synthesized materials. XRD and FTIR analyses showed that slow addition (0.5 mL/min) promoted the formation of highly crystalline, predominantly phase-pure fluorapatite (93%), while fast addition (5 mL/min) led to supersaturation-induced nucleation, facilitating the stabilization of whitlockite (61%). SEM analysis showed that the fluorapatite crystals were well-shaped and homogeneous, with little agglomeration at 0.5 mL/min. However, when the addition was accelerated, the particles formed irregular structures with greater agglomeration and structural heterogeneity.

Keywords: eggshells, fluorapatite, whitlockite, co-precipitation, precursor addition rate.

INTRODUCTION

The need for sustainable techniques for the recovery of secondary raw materials is influenced not only by the depletion of natural resources but also by the increasing amount of waste [1]. In recent years, there has been growing interest in developing sustainable methods for converting waste resources into high-value-added materials [1–3]. In this context, eggshells, mostly constituted of calcium carbonate, present a promising biogenic resource [4–5] for the synthesis of calcium phosphate minerals such as fluorapatite [6–8].

Fluorapatite is a material of increasing interest in biomedical sciences due to its combination of high mechanical stability and excellent biocompatibility. Compared to other calcium phosphate compounds, it exhibits superior resistance to dissolution [9], making it a preferred material for long-term applications in physiological environments. As a result, fluorapatite has been extensively investigated for use in bone tissue engineering [10–14] and dental applications [15–16], with the specific conditions associated with the different synthesis processes strongly influencing its structural and functional properties [17–19].

The chemical co-precipitation method stands out as an economically efficient and scalable approach for the synthesis of calcium-phosphate materials, in which calcium, phosphate, and fluoride ions are simultaneously precipitated in an aqueous solution. To achieve a pure fluorapatite phase, it is important to retain the stoichiometric ratio between the constituent ions. Nuzulia et al. [8] found that changing the P/F molar ratio significantly affects the formation of fluorapatite, which is reflected in changes in X-ray diffraction and phase purity. Furthermore, Iijima et al. [20] established that fluoride ions modulate the dynamics of the phase transition, affecting crystal growth and orientation, which provides opportunities for optimizing synthesis conditions.

Another critical parameter affecting the phase composition, particle size, and morphology of

the synthesized fluorapatite is the rate of fluoride precursor addition, which directly impacts the structural integrity and functional properties of the final material. In this context, the present study aimed to synthesize fluorapatite from waste eggshells as a source of biogenic calcium via the co-precipitation method. Evaluated how different rates of adding phosphorus–fluorine precursors (0.5 and 5 mL/min^{-1}) affect phase composition, crystal morphology, and structural characteristics. The resulting materials were characterized using XRD, FTIR, and SEM to establish correlations between precursor addition rate and the properties of the synthesized fluorapatite. The novelty of this work lies in combining the sustainable use of waste eggshells with a systematic investigation of the precursor addition rate, a factor which is not enough investigated in previous studies. This work will provide new data on its influence on the characteristics of the synthesized fluorapatite.

EXPERIMENTAL

Materials

Waste eggshells collected from a local confectionery, 0.3 M standard solution of orthophosphoric acid (H_3PO_4, 85%) and 0.1 M sodium fluoride solution (NaF, 99%), products of Sigma-Aldrich.

Pretreatment of eggshells and preparation of calcium hydroxide

Waste eggshells were washed several times with hot water without removing the organic membrane. They were then allowed to air dry at room temperature for 24 hours and at 105 °C until constant mass was reached. The dry shells underwent mechanically processed in a Fritsch "Pulverisette 6" planetary mill (at 300 rpm for 60 min, under dry conditions) to produce a fine powder. This powder was subsequently sieved using a Retsch "AS 200" vibrating shaker with laboratory sieves (ISO 33101, 100–25 μm) to determine the particle size distribution. The resulting eggshell powder underwent thermal treatment at 900 °C for 3 hours, to effectively decompose calcium carbonate ($CaCO_3$) into calcium oxide (CaO) [21]. Subsequently, the CaO powder was dissolved in the required amount of distilled water and stirred at 400 rpm for 15 min to form $Ca(OH)_2$, which serves as the calcium ion source.

Synthesis of fluorapatite

The synthesis of fluorapatite was carried out using the chemical co-precipitation method. A precursor solution was first prepared by mixing 0.3 M phosphoric acid (H_3PO_4) and 0.1 M sodium fluoride (NaF) solutions in a 1:1 volume ratio under continuous stirring at room temperature until a homogeneous solution was obtained. This phosphorus-fluoride precursor was then introduced into a calcium hydroxide ($Ca(OH)_2$) solution under magnetic stirring (200 rpm) at 25 °C. The synthesis was performed with two distinct addition rates: 0.5 mL/min (slow) and 5 mL/min (fast). The molar Ca/P ratio was maintained at 1.67, with a final Ca:P:F ratio of 5:3:1[18], corresponding to the stoichiometry of fluorapatite [$Ca_5(PO_4)_3F$].

Since solution pH is a key factor governing the formation of fluorapatite and crystal growth, its change during synthesis was monitored. The initial pH of the $Ca(OH)_2$ solution was approximately 12. The rate of addition had a significant impact on the pH dynamics during precipitation. The slow addition (0.5 mL/min) resulted in a gradual and uniform decrease in pH to values between 9 and 10. In contrast, the fast addition (5 mL/min) caused a sharp decrease, with transient values of 8–9 and noticeable local acidification at the injection point. Despite these differences, the reaction environment remained alkaline (pH > 7) throughout the process in both cases, which is within the optimal range for apatite formation.

After the complete addition of the precursor, the suspension was aged for 24 hours at room temperature. The resulting precipitate was separated by vacuum filtration, washed with distilled water, and the collected powder was dried at 70 °C for 24 hours. Finally, the powder was calcined at 750 °C for 2 hours with a heating rate of 5 °C/min. This calcination temperature was selected to enhance the crystallinity and phase purity of the fluorapatite while avoiding decomposition or the formation of secondary phases, such as CaO or CaF_2, which typically occur at temperatures above 800 °C. The experimental procedures are presented in the flow chart shown in Figure 1.

Characterization

X-ray diffraction (XRD) characterization was employed to determine the phase purity and of the obtained powders using a powder diffractometer

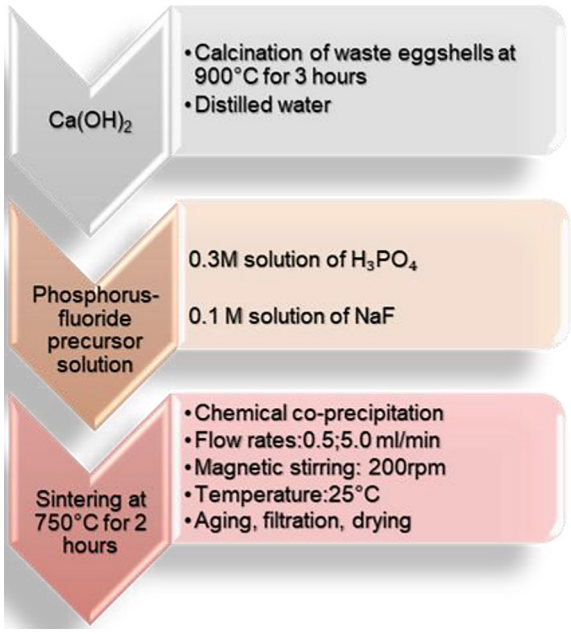

Figure 1. Flow chart of fluorapatite synthesis

Bruker 2D Phaser. The samples were irradiated with CuKα radiation (λ = 1.54060 Å) and analyzed between 2–90° (2 theta). Samples were also characterized by Fourier transform infrared (FT-IR) Nicolet iS 50 FT-IR Thermo Scientific to identify the functional groups of the samples. Analysis is performed in the interval 4000–400 cm^{-1}. To observe the surface morphology of the samples Scanning electron microscopy was performed on a JSM 6390 electron microscope (Japan) in conjunction with energy dispersive X-ray spectroscopy (EDS, Oxford IN-CA Energy 350) equipped with an ultrahigh resolution scanning system (ASID-3D) in regimes of secondary electron image and back scattered electron image.

RESULTS AND DISCUSSION

To ensure the quality and reactivity of the calcium hydroxide for the synthesis of fluorapatite, ground eggshells were subjected to granulometric (fractional) analysis. The purpose of the analysis was to determine the particle size distribution and to identify a suitable fraction for subsequent thermal treatment. The results indicated that the dominant particle fraction, accounting for 68.1% of the total mass, was retained on a sieve with a mesh size of 32 µm (Figure 2). According to our previous investigation [22], this size of particles exhibited a specific surface area of 3.6654 m^2/g and a total porosity of 0.0064 cm^3/g, parameters that make it extremely suitable for further calcination. The relatively high specific surface area enhances the number of reactive sites available for CO_2 desorption, thereby accelerating the thermal decomposition of $CaCO_3$ to CaO and ensuring a more uniform conversion throughout the particle bulk [23]. Simultaneously, the porosity of 0.0064 cm^3/g facilitates the diffusion of evolved gaseous products (primarily CO_2) from the interior to the surface, minimizing pore blockage, thus preserving reactivity and surface accessibility during calcination. The selected particle fraction was subjected to calcination at 900 °C for 3 hours, conditions chosen based on literature that emphasize the role of elevated temperature and prolonged thermal exposure in enhancing the phase purity and crystallinity of the resulting calcium oxide (CaO) [24–25].

X-ray diffraction analysis was performed to determine the crystalline phases present in the synthesized powders obtained at different precursor addition rates. The experimental diffraction peaks were indexed and matched to standard reference data from the Crystallography Open Database (COD). As presented in Figure 3, for the sample synthesized at a 0.5 mL/min^{-1} addition rate of a precursor, the X-ray diffraction pattern is dominated by sharp, high-intensity peaks at 2θ angles of 25.9°, 31.8°, 32.9°, 34.0°, and 39.8°. These reflections correspond to the (002), (211), (300), (202), and (310) lattice planes of fluorapatite ($Ca_5(PO_4)_3F$), confirming a well-crystallized apatite phase.

The most intense and characteristic peak was found at 2θ = 31.8°, indexed to the (211) plane of fluorapatite, and aligns precisely with established fluorapatite patterns [26]. The relative intensities and narrow peak widths are consistent with previously reported XRD patterns of well-ordered fluorapatite synthesized under controlled precipitation conditions and consistent with COD 9017795. In addition to the primary fluorapatite phase, minor secondary reflections are observed at 2θ angles of 29.4°, 31.0°, and 34.5°, corresponding to the (300), (021), and (113) planes of whitlockite (COD 9011161), suggesting trace amounts of a whitlockite-type structure ($Ca_9Mn(HPO_4)(PO_4)_6$). The relatively low intensity of these reflections confirms that fluorapatite remains the main crystalline phase, with whitlockite present only as a minor impurity.

The sample synthesized at addition rates of 5 mL/min^{-1} (Figure 4), showed a clear change in

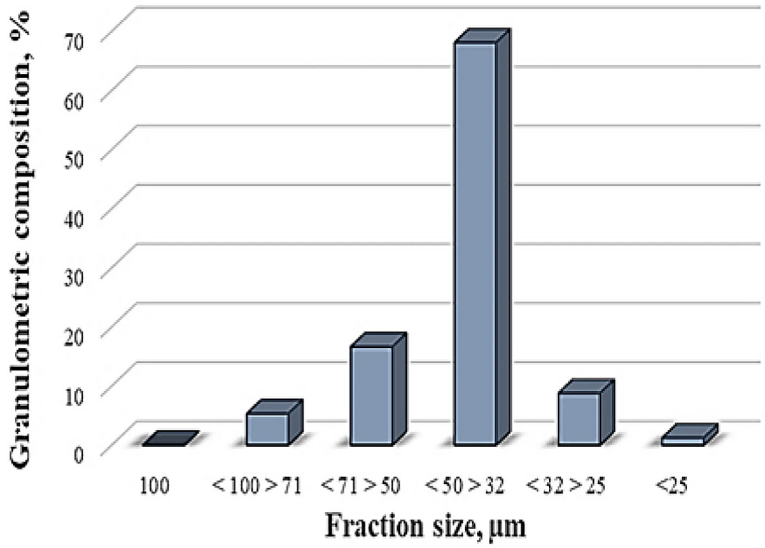

Figure 2. Fractional composition of waste eggshells

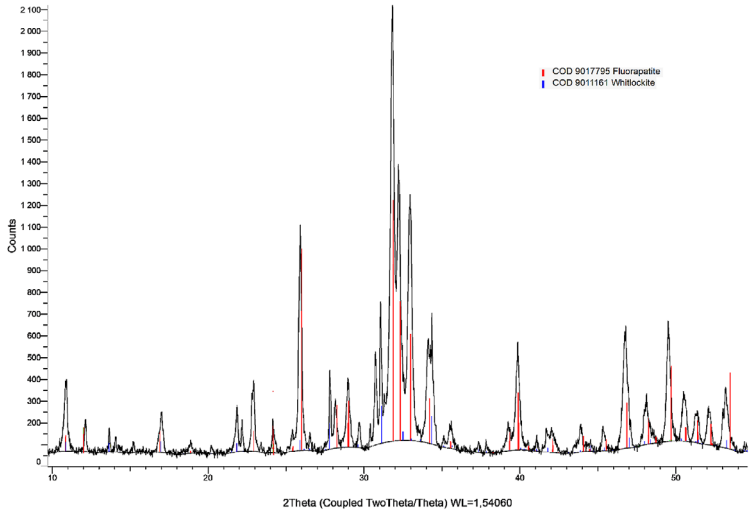

Figure 3. XRD diffractogram of sample obtained at 0.5 mL/min addition rate

the composition of the phases. The main reflections were between 2θ = 27° and 35°, with the strongest peaks at about 30.9°, 31.1°, and 34.5°. These peaks correspond to manganese whitlockite ($Ca_9Mn(HPO_4)(PO_4)_6$, which is consistent with COD reference pattern 9011161. In the higher-angle region (2θ > 40°), there were more low-intensity peaks for whitlockite, such as reflections at 40.1°, 41.1°, 41.5°, 46.9°, 48.3°, and 53.4°. Although fluorapatite reflections remain detectable particularly at 2θ=25.9°, 31.8°, and 39.8°, their relative intensities are markedly reduced compared to the slow-addition rate sample. This suggests that fluorapatite persists as a secondary phase under fast addition conditions, where the dominant crystallization pathway shifts toward whitlockite-type structures due to the increased rate of ion supersaturation.

The X-ray diffraction results clearly show the influence of the rate of addition of phosphorus-fluoride precursor into calcium solution (derived from eggshells) on the formation of crystalline phases in the obtained materials. Figure 5 presents their quantitative distribution determined by the instrument's software (Bruker 2D Phaser) based on the intensity and profile of the diffraction peaks. It was observed that at a slow addition rate (of 0.5 mL/min^{-1}), the samples consist of 93% fluorapatite ($Ca_5(PO_4)_3F$) and only 7% whitlockite ($Ca_9Mn(HPO_4)(PO_4)_6$), while at a fast addition of precursor (at 5 mL/min^{-1}), the phase balance shifts towards 61% whitlockite and 39%

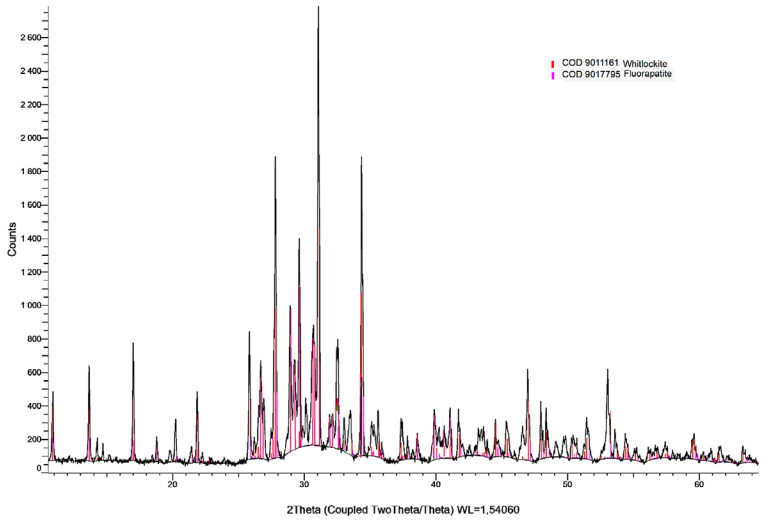

Figure 4. XRD diffractogram of sample obtained at 5 mL/min addition rate

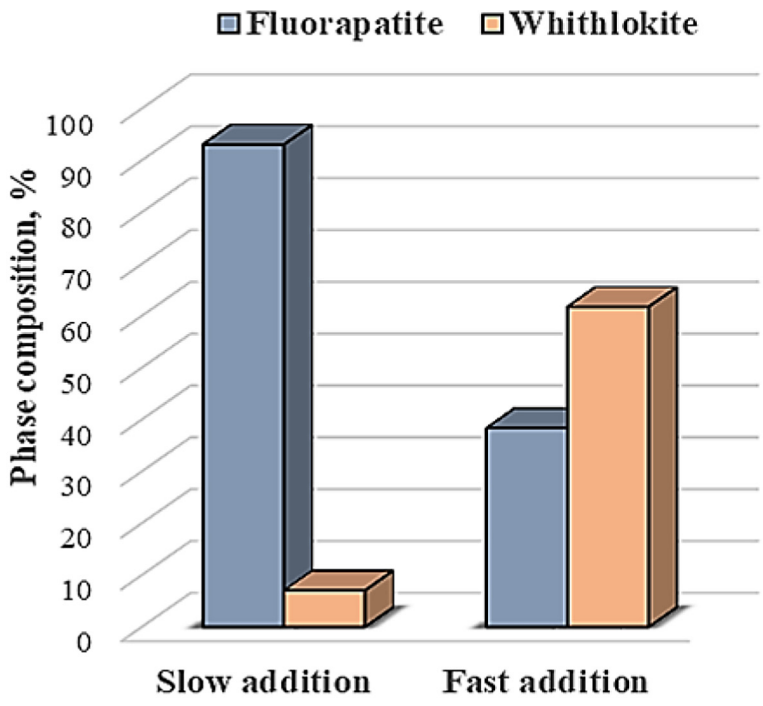

Figure 5. Phase composition of synthesized materials

fluorapatite. This phase evolution is due to the differences in the kinetics of supersaturation and nucleation [27]. With slow addition, the ion concentrations in the solution are gradually raised, maintaining low supersaturation and allowing the formation of fewer, but thermodynamically stable, nuclei [28]. These conditions favor the crystallization of fluorapatite with a well-defined lattice arrangement, as evidenced by the sharp reflections in the diffraction patterns corresponding to the (002), (211), and (300) planes [26]. The minor whitlockite reflections detected at this stage may be due to residual, metastable nuclei that did not fully transform during the 24-h aging period, persisting as a secondary phase.

In contrast, a fast addition rate of precursor creates transient supersaturation peaks, leading to massive homogeneous nucleation and the formation of multiple small, metastable nuclei [27, 29]. This competitive environment limits crystal growth and inhibits the structural ordering required for apatite formation, instead stabilizing whitlockite, which can readily incorporate divalent cations such as Mn^{2+} and Mg^{2+} into its lattice

[30]. Importantly, the presence of manganese is directly related to the eggshell-derived precursor, as trace amounts of Mn^{2+} ions, naturally occurring in biogenic eggshell, act as lattice stabilizers during whitlockite formation. Furthermore, the absence of other calcium phosphate phases, such as monetite ($CaHPO_4$) or brushite ($CaHPO_4$ $2H_2O$), is consistent with the alkaline conditions provided by $Ca(OH)_2$ (pH > 7) and the relatively high Ca/P molar ratio (>1.5). Stabilization of a single apatite phase under such conditions has a direct impact on the purity of the phase, which in turn determines the crystallite size, morphology and overall homogeneity of the final material. As a result, the synthesis process becomes highly sensitive to parameters such as reagent addition rate, pH and temperature, as documented in wet precipitation method using eggshell-derived precursors [7, 9].

Fourier-transform infrared spectroscopy (FTIR) was used to characterize the materials obtained based on the rate of phosphorus-fluoride precursor addition to the calcium ion solution derived from eggshells. Table 1 summarizes the FTIR spectral characteristics of the synthesized powders, while Figure 6 presents the FTIR spectra corresponding to the various precursor addition rates. Both spectra show characteristic infrared absorption bands typical of phosphate-containing compounds, with notable differences in bands intensity, shape, and spectral resolution.

The main intense peak in the 1030–1100 cm^{-1} region is attributed to the asymmetric stretching vibration $\nu_3(PO_4^{3-})$, while the bands around 960cm^{-1} correspond to the symmetric stretching vibration $\nu_1(PO_4^{3-})$. The pair of well-defined peaks in the 560–605 cm^{-1} range reflects the deformation modes $\nu_4(PO_4^{3-})$, characteristic of well-organized phosphate tetrahedra [30]. In the sample synthesized with precursor addition of 0.5 mL/min^{-1}, these vibrational modes are clearly expressed with sharp and narrow peaks, indicating a high degree of crystallinity and the dominance of the fluorapatite phase ($Ca_5(PO_4)_3F$), as confirmed by XRD analysis. In addition to the characteristic phosphate absorptions, the sample obtained by slow addition of the precursor shows a weak but distinct FTIR band near 3570 cm^{-1}. Although this frequency often corresponds to stretching of the OH^- group [31], its retention after calcination at 750 °C and cooling does not suggest the presence of structurally bound hydroxyl groups or organic residues. The observed band is therefore the result of surface adsorbed moisture (H_2O), which is bound by hydrogen bonds to active surface sites or defects in the crystal lattice. Adsorbed water in apatite materials typically shows absorption in the region of approximately 3100–3600 cm^{-1}, sometimes

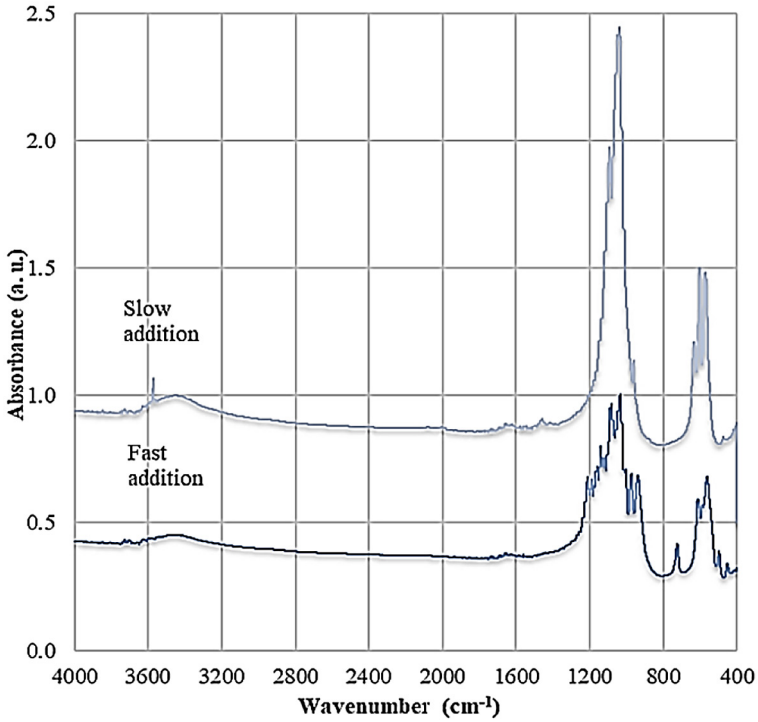

Figure 6. FT–IR spectra of synthesized materials obtained at different precursor addition rate

Table 1. FTIR spectral characteristics of synthesized materials at different precursor addition rates

Wavenumber (cm^{-1})	Vibrational mode group	0.5 mL/min^{-1} slow addition	5 mL/min^{-1} fast addition	Interpretation
~1030–1100	$v_3(PO_4^{3-})$, asymmetric stretching	Sharp, well-defined high-intensity band	Broader	Higher crystallinity under slow addition; structural disorder at fast rate
~960	$v_1(PO_4^{3-})$, symmetric stretching	Clearly visible and sharp peak	Weaker and less defined	Indicates dominant fluorapatite in slow addition sample
~560–605	$v_4(PO_4^{3-})$, bending modes	Distinct doublet	Resolved shoulder	Better phosphate tetrahedra organization under slow addition
~875–880	$v(HPO_4^{2-})$, protonate phosphate	Very weak	More intense and pronounced	Suggests whitlockite-type phase under fast addition
~3570	v(OH), surface-adsorbed water	Weak, narrow band	Absent	Attributed to re-adsorbed moisture post-calcination; not structural OH^-

manifesting as a sharper peak around 3570 cm^{-1}. The presence of such physically adsorbed water is consistent with observations of Gheisari et al. [32] re-adsorption of water upon exposure to ambient air after thermal treatment.

The FTIR spectrum of the sample synthesized at a 5 mL/ min^{-1} precursor addition rate is significantly different. The PO_4^{3-} vibrational modes in the region 1000–1100 cm^{-1} (v_3) and 560–610 cm^{-1} (v_4), are broadened and with lower intensity, which is indicative of a lower degree of crystallinity and the presence of mixed calcium-phosphate phases. A distinct and enhanced band at 875–880 cm^{-1} is observed, which is characteristic of protonated phosphate groups (HPO_4^{2-}), together with an additional peak below 800 cm^{-1}, which can be attributed to structural disorder induced by protonated phosphates [33]. The presence of manganese promotes the stabilization of whitlockite by substituting Ca^{2+} at octahedral sites, thereby influencing both the crystal chemistry and vibrational characteristics of the phase [34].

Scanning electron microscopy (SEM) analysis was used to investigate the morphological characteristics of the synthesized calcium phosphate powders, and the results are presented in Figures 7 and 8. SEM images show a direct correlation between the reagent addition rate and the resulting particle morphology, size distribution, and degree of agglomeration, which is further confirmed by the XRD phase composition data. Figure 7 present the morphology of the sample synthesized at a slow addition rate of 0.5 mL/ min^{-1}. Well-formed, homogeneous crystals with a distinct apatite morphology are observed, which correlates with the dominant fluorapatite phase identified by XRD. The particles show a narrow size distribution from 1–2 μm, and low agglomeration tendency, with clear boundaries between individual crystals. This highly homogeneous and ordered microstructure is the result of controlled crystallization kinetics. The slow addition rate of reagents minimizes local fluctuations in supersaturation, allowing for a lower nucleation density. Consequently, a smaller number of stable nuclei are formed and undergo sustained growth under near-equilibrium conditions, facilitated by sufficient time for ion diffusion and incorporation into the crystal lattice. This leads to the development of large, thermodynamically stable crystals with high phase purity, which is consistent with the XRD results identifying fluorapatite as the predominant (93%) phase.

The sample obtained at an addition rate of 5 mL/min^{-1} (Figure 8) exhibits a different morphology. The microstructure is highly heterogeneous, consisting of irregular aggregates with a rough surface texture, a high degree of agglomeration and a size of 3–5 μm. This reflects a more chaotic nucleation and competition between fluorapatite and whitlockite, driven by the fast addition rate, leading to local supersaturation of homogeneous nucleation, generating a large number of metastable primary particles. In order to minimize their surface energy, these particles undergo fast and uncontrolled agglomeration, forming the observed large agglomerates. The formation of whitlockite together with fluorapatite further disrupts the morphological homogeneity and contributes to the complex, aggregated structure observed in the SEM micrograph.

The pronounced agglomeration observed in the sample prepared at an addition rate of 5 mL/ min^{-1} was likely intensified by the subsequent

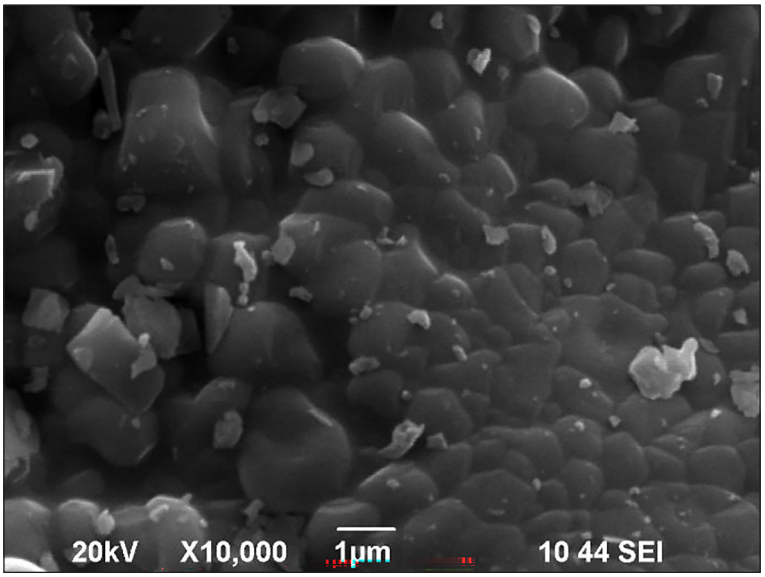

Figure 7. SEM micrograph of the calcium phosphate powder synthesized at a 0.5 mL/min precursor addition rate

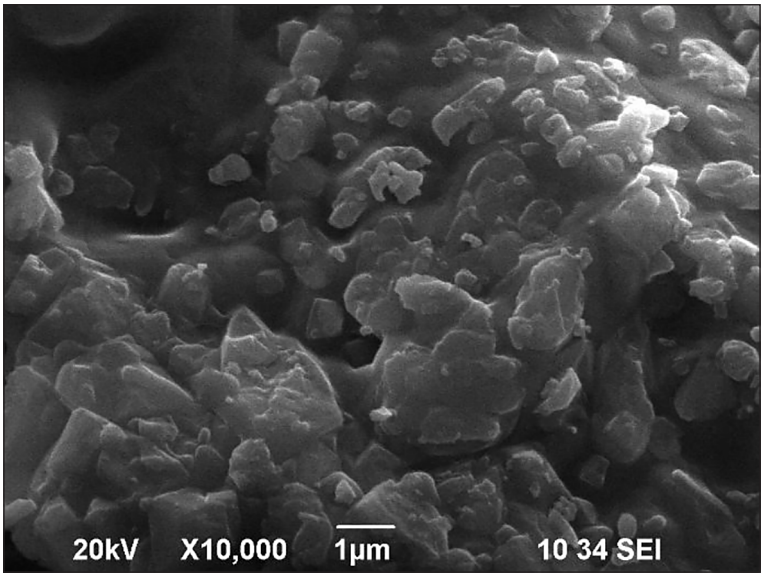

Figure 8. SEM micrograph of the calcium phosphate powder synthesized at a 5 mL/min precursor addition rate

heat treatment at 750 °C. At elevated temperatures, sintering promotes particle coalescence, thereby increasing morphological heterogeneity in the final microstructure [26]. In contrast, the sample obtained at the slower addition rate of 0.5 mL/min^{-1} exhibited reduced agglomeration. In this case, firing at 750 °C favored the formation of phase-pure fluorapatite with well-defined crystal morphology [7].

Energy-dispersive X-ray spectroscopy (EDS) analysis was performed to quantify the elemental composition and Ca/P ratios of the samples (Table 2). EDS confirmed the presence of Ca, P, O, and F as the major elements, in agreement with the fluorapatite structure. In the sample synthesized at a slow precursor addition rate (0.5 mL/min), the Ca/P atomic ratio obtained from EDS was 1.69, very close to the theoretical value of 1.67 for stoichiometric fluorapatite, and no Mn was detected. In contrast, the sample prepared at a fast addition rate (5 mL/min) exhibited a lower Ca/P ratio of 1.49, consistent with the increased whitlockite content revealed by XRD, along with trace Mn (1.2 at.%) incorporated into the whitlockite lattice. These findings are in agreement with previous studies showing that the Ca/P ratio of fluorapatite typically ranges from 1.56 to 1.67 depending on fluoride incorporation

Table 2. EDS elemental composition of synthesized samples

Addition rate sample	Ca (at.%)	P (at. %)	O (at. %)	F (at. %)	Mn (at. %)	Ca/P ratio
0.5 mL/min (93% Fluorapatite)	36.8	21.7	40.0	1.5	Not detected	1.69
5 mL/min (39% Fluorapatite 61% Whitlockite)	34.2	23.0	40.6	1.0	1.2	1.49

[35], and that deviations towards lower values reflect stabilization of secondary calcium phosphate phases [36].

CONCLUSIONS

This work demonstrates that rate of precursor addition is a critical factor influencing the synthesis of fluorapatite from a renewable biogenic source – waste eggshells. Using a co-precipitation method, we showed that there is a direct correlation between the addition rate, the solution's degree of supersaturation, and the resulting phase composition and microstructure. It was found that a slow, controlled addition rate (0.5 mL/min) maintained low supersaturation, which preferentially directed crystallization towards the formation of phase-pure, well-crystalline fluorapatite (93%) with a well-defined morphology and minimal agglomeration. A fast addition rate (5 mL/min) induced sharp supersaturation peaks, triggering competing nucleation pathways that led to the stabilization of whitlockite (61%) as the dominant phase. This sample was characterized by lower crystallinity, structural disorder, and significant morphological heterogeneity with pronounced agglomeration.

The study finds that the precursor addition rate is a simple but effective way to change the phase composition, purity, and microstructural properties of calcium phosphate materials. The research not only has scientific value, but it also shows how biogenic calcium sources can be used in a sustainable way transform waste eggshells into high-value functional biomaterials. These materials are important for biomedical uses like bone tissue engineering and dental restoration, where phase purity and a controlled microstructure are important for long-term performance. Furthermore, the tunable surface properties and chemical stability of the synthesized calcium phosphates suggest potential for environmental applications, such as catalytic supports or adsorbents for wastewater remediation.

Acknowledgement

This work was supported by the Scientific Research Center at Burgas State University under the contract № 495/2024.

REFERENCES

1. Arun M., Barik D., Chandran S. Exploration of material recovery framework from waste – A revolutionary move towards clean environment. Chem. Eng. J. Adv. 2024; 18: 100589. https://doi.org/10.1016/j.ceja.2024.100589
2. Sultana I., Chen Y., Huang S., Rahman M. Recycled value-added circular energy materials for new battery application: Recycling strategies, challenges, and sustainability-a comprehensive review. J. Environ. Chem. Eng. 2022; 10(6): 108728. https://doi.org/10.1016/j.jece.2022.108728
3. Francis A. Ecologic and economic motives for transforming calcium-based food wastes into sustainable value-added products: a review. Environ. Sci. Pollut. Res. 2024; 32(2): 428–451.
4. https://doi.org/10.1007/s11356-024-35649-w
5. Azarian M., Sutapun W. Biogenic calcium carbonate derived from waste shells for advanced material applications: A review. Front. Mater. 2022; 9. https://doi.org/10.3389/fmats.2022.1024977
6. Jayasree R., Madhumathi K., Rana D., Ramalingam M., Nankar R., Doble M., Kumar T. Development of egg shell derived carbonated apatite nanocarrier system for drug delivery. J. Nanosci. Nanotechnol. 2018; 18(4): 2318–2324. https://doi.org/10.1166/jnn.2018.14377
7. Kalbarczyk M., Szcześ A., Kantor I., May Z., Sternik, D. Synthesis and Characterization of calcium phosphate materials derived from eggshells from different poultry with and without the eggshell membrane. Mater. 2022; 15(3): 934. https://doi.org/10.3390/ma15030934
8. Kareem Z., Eyiler E. Synthesis of hydroxyapatite from eggshellsviawet chemical precipitation: a review. RSC Adv. 2024; 14(30): 21439–21452. https://doi.org/10.1039/d4ra02198c
9. Nuzulia N., Sari Y., Sari D. Synthesis of Duck Eggshells-based Fluorapatite by Using Microwave

Irradiation. In: 1st International Conference on Bioinformatics, Biotechnology, and Biomedical Engineering - Bioinformatics and Biomedical Engineering; October; 2018. https://doi.org/10.1109/biomic.2018.8610626

10. Seyedmajidi S., Seyedmajidi M., Fluorapatite: A review of synthesis, properties and medical applications vs hydroxyapatite. Iran. J. Mater. Sci. Eng. 2022; 19(2): 1–20.
11. http://ijmse.iust.ac.ir/article-1-2430-en.html
12. Malysheva K., Kwaśniak K., Gnilitskyi I., Barylyak A., Zinchenko V., Fahmi A., Korchynskyi O., Bobitski Y. Functionalization of polycaprolactone electrospun osteoplastic scaffolds with fluorapatite and hydroxyapatite nanoparticles: biocompatibility comparison of human versus mouse mesenchymal stem cells. Mater. 2021: 14(6); 1333. https://doi.org/10.3390/ma14061333
13. Denry I., Goudouri O., Harless J., Holloway J. Rapid vacuum sintering: A novel technique for fabricating fluorapatite ceramic scaffolds for bone tissue engineering. J. Biomed. Mater. Res. B: Appl. Biomater. 2017: 106(1); 291–299. https://doi.org/10.1002/jbm.b.33825
14. Jeyapalina S., Hillas E., Beck J., Agarwal J., Shea J. Fluorapatite and fluorohydroxyapatite apatite surfaces drive adipose-derived stem cells to an osteogenic lineage. J. Mech. Behav. Biomed. Mater. 2022: 125; 104950. https://doi.org/10.1016/j.jmbbm.2021.104950
15. Santiago E., Martin V., Colaço B., Fernandes M., Santos C., Gomes P. Hydrothermal synthesis of fluorapatite coatings over titanium implants for enhanced osseointegration—an in vivo study in the rabbit. J. Funct. Biomater. 2022: 13(4); 241. https://doi.org/10.3390/jfb13040241
16. Borkowski L., Przekora A., Belcarz A., Palka K., Jozefaciuk G., Lübek T., Jojczuk M., Nogalski A., Ginalska G. Fluorapatite ceramics for bone tissue regeneration: Synthesis, characterization and assessment of biomedical potential. Mater. Sci. Eng. C. 2020; 116: 111211.
17. https://doi.org/10.1016/j.msec.2020.111211
18. Pajor K., Pajchel L., Kolmas J. Hydroxyapatite and fluorapatite in conservative dentistry and oral implantology – a review. Mater. 2019: 12(17); 2683. https://doi.org/10.3390/ma12172683
19. Nuzulia N., Bachtiar E., Alisyah D., Widya Sari Y. Synthesis of nano-fluorapatite and their biocompatibility test as restorative dental materials. AIP Conference Proceedings; 2024. https://doi.org/10.1063/5.0227909
20. Taheri M., Rezazadeh Shirdar M., Keyvanfar A., Shafaghat A. Evaluating hydrothermal synthesis of fluorapatite nanorods: pH and temperature. J. Exp. Nanosci. 2016: 12(1); 83–93.
21. https://doi.org/10.1080/17458080.2016.1263400
22. Charlena C., Sari Y., Islamia W. Variation of sintering temperature in the synthesis of fluorapatite from snail shells (*Achatina fulica*) using the sol-gel method. Indones. J. Pure Appl. Chem. 2023: 6(3); 152.
23. https://doi.org/10.26418/indonesian.v6i3.67697
24. Chaikina M., Bulina N., Prosanov I., Ishchenko A. Formation of fluorapatite in the equilibrium system $CaO–P_2O_5–HF–H_2O$ at 298 K in a nitrogen atmosphere. Cryst. 2023: 13(8); 1264.
25. https://doi.org/10.3390/cryst13081264
26. Iijima M., Onuma K. Roles of fluoride on octacalcium phosphate and apatite formation on amorphous calcium phosphate substrate. Cryst. Growth Des. 2018: 18(4); 2279–2288. https://doi.org/10.1021/acs.cgd.7b01717
27. Asra D., Sari Y., Dahlan K. Effect of Microwave Irradiation on the Synthesis of Carbonated Hydroxyapatite (CHA) from Chicken Eggshell. IOP Conf. Ser.: Earth Environ.Sci.; 2018. https://10.1088/1755-1315/187/1/012016
28. Kiryakova D., Kolchakova G. Preparation and characterization of eggshells powders treated with hydrochloric acid and sodium hydroxide. Adv. Eng. Lett. 2023: 3; 81–87. https://doi.org/adeletters.2023.2.3.1
29. Adaikalam K., Hussain S., Anbu P., Rajaram A., Sivanesan I., Kim H. Eco-friendly facile conversion of waste eggshells into CaO nanoparticles for environmental applications. Nanomater. 2024: 14(20); 1620. https://doi.org/10.3390/nano14201620
30. Bayram N., Dikmen S., Malkoç S. Effect of different calcination temperatures on synthesized hydroxyapatites from waste eggshell. Eskişehir Technical University J. Sci Technol. A Appl. Sci. Eng. 2024: 25(4); 590–601. https://doi.org/10.18038/estubtda.1539308
31. Chuakham S., Putkham A., Chaiyachet Y., Saengprajak A., Banlue K., Tanpaiboonkul N., Putkham, A. Scalable production of bio-calcium oxide via thermal decomposition of solid - hatchery waste in a laboratory-scale rotary kiln. Sci. Rep. 2025:15(1); 865.
32. https://doi.org/10.1038/s41598-024-84889-w
33. Khofiyatuzziyadah A., Charlena C., Maddu A. Synthesis and characterization of golden snail shell-based fluorapatite via precipitation and solid-state reaction methods. Mater. Int. 2024: 6(4); 32.
34. https://doi.org/10.33263/Materials64.032
35. Kashchiev A. Nucleation: basic theory with applications. 2000. Butterworth Heinemann.
36. Perepezko J. Nucleation-controlled reactions and metastable structures. Prog. Mater. Sci. 2004: 49(3–4); 263–284. https://doi.org/10.1016/s0079-6425(03)00028-8

37. Wu W., Nancollas G. Kinetics of nucleation and crystal growth of hydroxyapatite and fluorapatite on titanium oxide surfaces. Colloids Surf B: Biointerfaces. 1997: 10(2); 87–94.
38. https://doi.org/10.1016/S0927-7765(97)00054-4
39. Capitelli F., Bosi F., Capelli S., Radica F., Della Ventura G. Neutron and XRD single-crystal diffraction study and vibrational properties of whitlockite, the natural counterpart of synthetic tricalcium phosphate. Cryst. 2021: 11(3);225. https://doi.org/10.3390/cryst11030225
40. Bulina N., Makarova S., Prosanov I., Vinokurova O., Lyakhov N. Structure and thermal stability of fluorhydroxyapatite and fluorapatite obtained by mechanochemical method. J. Solid State Chem. 2020: 282; 121076. https://doi.org/10.1016/j.jssc.2019.121076
41. Gheisari H., Karamian E., Abdellahi M. A novel hydroxyapatite –Hardystonite nanocomposite ceramic. Ceram. Int. 2015: 41(4); 5967-5975. http://dx.doi.org/10.1016/j.ceramint.2015.01.033
42. Cooper M., Hawthorne F., Abdu Y., Ball N., Ramik, R., Tait K. Wopmayite, ideally $Ca_6Na_3Mn(PO_4)_3(PO_3OH)_4$, a new phosphate mineral from the Tanco Mine, Bernic Lake, Manitoba. Can. Mineral. 2013: 51; 93–106. https://doi.org/10.3749/canmin.51.1.93
43. Zhao J., Jing Q., Zhou T., Zhang X., Li, W., Pang, H. Controllable synthesis of manganese organic phosphate with different morphologies and their derivatives for supercapacitors. Mol. 2024: 29(17); 4186. https://doi.org/10.3390/molecules29174186
44. Rodríguez-Lorenzo L., Hart J., Gross K. Structural and chemical analysis of well-crystallized hydroxy-fluorapatites. J. Phys. Chem. B. 2003: 107(33); 8316–8320. https://doi.org/10.1021/JP027556O
45. Moisescu C., Höche T., Carl G., Keding R., Rüssel C., Heerdegen W. Influence of the Ca/P ratio on the morphology of fluorapatite crystals in SiO_2–Al_2O_3–CaO–P_2O_5–K_2O–F− glass-ceramics. J. Non-Cryst. Solids. 2001: 289(1), 123–134. https://doi.org/10.1016/S0022-3093(01)00712-8